arXiv:1202.3659v1 [cond-mat.mes-hall] 16 Feb 2012

Optomechanical circuits for nanomechanical continuous variable quantum state processing

Michael Schmidt,[1] Max Ludwig,[1] and Florian Marquardt[1,2]
[1] *Friedrich-Alexander-Universität Erlangen-Nürnberg, Staudtstr. 7, D-91058 Erlangen, Germany*
[2] *Max Planck Institute for the Science of Light, Günther-Scharowsky-Straße 1/Bau 24, D-91058 Erlangen, Germany*

We propose and analyze a nanomechanical architecture where light is used to perform linear quantum operations on a set of many vibrational modes. Suitable amplitude modulation of a single laser beam is shown to generate squeezing, entanglement, and state-transfer between modes that are selected according to their mechanical oscillation frequency. Current optomechanical devices based on photonic crystals may provide a platform for realizing this scheme.

The field of cavity optomechanics studies the interaction between light and nanomechanical motion, with promising prospects in fundamental tests of quantum physics, ultrasensitive detection, and applications in quantum information processing (see [1] for a review). One particularly promising platform consists of "optomechanical crystals", with strongly localized optical and vibrational modes implemented in a photonic crystal structure [2]. So far, several interesting possibilities have been pointed out that would make use of multi-mode setups that can be designed on this basis. For example, suitably engineered setups may coherently convert phonons to photons [3] and collective nonlinear dynamics might be observed in optomechanical arrays [4]. Moreover, optomechanical systems in general have been demonstrated to allow writing quantum information from the light field into the long-lived mechanical modes [5–7]. The recent success in ground state laser-cooling [8] has now opened the door to coherent quantum dynamics in optomechanical systems.

In this paper, we propose a general scheme for continuous-variable quantum state processing [9] utilizing the vibrational modes of such structures. We will show how entanglement and state transfer operations can be applied selectively to pairs of modes, by suitable intensity modulation of a single incoming laser beam. We will discuss the limitations for entanglement generation and transfer fidelity, and show how to engineer the mechanical frequency spectrum and pick suitable designs to address these challenges.

Model. – We will first restrict our attention to a single optical mode coupled to many mechanical modes, such that the following standard optomechanical Hamiltonian describes the photon field $\hat{a}$, the phonons $\hat{b}_l$ of different localized vibrational modes ($l = 1, 2, \ldots, N$), and their mutual coupling:

$$\hat{H} = -\hbar\Delta\hat{a}^\dagger\hat{a} + \sum_l \hbar\Omega_l\hat{b}_l^\dagger\hat{b}_l - \hbar\hat{a}^\dagger\hat{a}\sum_l g_0^{(l)}(\hat{b}_l^\dagger + \hat{b}_l) + \ldots . \quad (1)$$

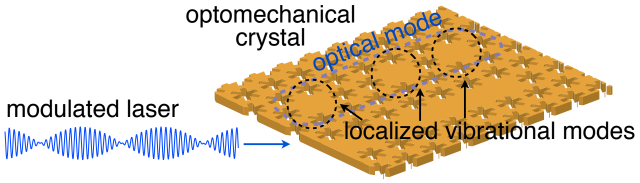

Figure 1: Schematic setup figure illustrating an optomechanical crystal with localized vibrational modes, coupled by a common optical mode. The optical mode is driven by an amplitude-modulated laser beam to engineer frequency-selective entanglement, squeezing and state-transfer operations of vibrations, as explained in the main text.

Here we are working in a frame rotating at the laser frequency, with the detuning given by $\Delta = \omega_L - \omega_{\rm cav}$. We omitted to explicitly write down the laser driving, and the coupling to the photon and phonon baths, with damping rates κ and Γ, respectively, although these will of course be taken care of in our treatment. The bare (single-photon) coupling constants $g_0^{(l)}$ depend on the overlap between the optical and mechanical mode functions. They are generally on the order of $\omega_{\rm cav}x_{\rm ZPF}/L$, where L is an effective optical cavity length that reaches down to wavelength dimensions in photonic crystal cavities, and where $x_{\rm ZPF} = (\hbar/2m_l\Omega_l)^{1/2}$ is the mechanical zero-point amplitude of the respective mode (see Fig. 1 for the illustration of a setup). After going through the standard procedure of splitting off the coherent optical amplitude induced by the laser, $\hat{a} = \alpha + \delta\hat{a}$, and omitting terms quadratic in $\delta\hat{a}$ (valid for strong drive), we recover the linearized optomechanical coupling,

$$\hat{H}_{\rm int} = -\hbar(\delta\hat{a}+\delta\hat{a}^\dagger)\sum_l g_l(\hat{b}_l^\dagger+\hat{b}_l) = -\hbar(\delta\hat{a}+\delta\hat{a}^\dagger)\hat{Y}. \quad (2)$$

Here the dressed couplings $g_l = g_0^{(l)}\alpha$ can be tuned via the laser intensity, i.e. the circulating photon number: $|\alpha| = \sqrt{\bar{n}_{\rm phot}}$, where we have taken α to be real-valued without loss of generality. We can now eliminate the driven cavity field (noting that $\delta\hat{a}$ is in the ground state) by second-order perturbation theory. Provided we work at large detuning, $|\Delta| \gg \Omega_l, \kappa$, we retain a fully coherent, light-induced mechanical coupling between all the modes,

$$\hat{H}^{\mathrm{eff}}_{\mathrm{int}} = \hbar \frac{\hat{Y}^2}{\Delta} = 2\hbar \sum_{l,k} J_{lk} \hat{X}_l \hat{X}_k \,, \tag{3}$$

where $\hat{X}_l \equiv \hat{b}_l + \hat{b}_l^\dagger$ is the mechanical displacement in units of x_{ZPF}. Eq. (3) may be viewed as a "collective optical spring" effect, coupling all the mechanical displacements. The couplings $J_{lk} = g_l g_k / 2\Delta$ can be changed in-situ either via the laser intensity or the detuning. Note that if multiple optical modes are driven, the corresponding coupling constants will add.

In general, the couplings in Eq. (3) will induce quantum state transfer between mutually resonant mechanical modes, and entanglement at low temperatures (usually with the help of optomechanical laser cooling). These phenomena have been analyzed in a variety of schemes [10–14] so far, typically with two mechanical modes of interest.

General scheme. – However, here we have in mind a multi-mode situation for continuous variable quantum information processing. To this end, we are interested in having an efficient approach to selectively couple arbitrary pairs of modes, both for entanglement and state transfer. There are several desiderata to address for a suitable optomechanical architecture of that style : (i) The couplings should be switchable in a time-dependent manner; (ii) one should be able to easily select pairs for operations; (iii) preferably, only one laser (or a limited number) should be involved; (iv) operation speeds should be large enough to overcome the effects of decay and decoherence; (v) one should be able to scale to a reasonably large number of modes.

Static couplings as in Eq. (3) could be used for selective pairwise operations if one were able to shift locally the mechanical mode frequency, to bring into resonance only the two respective modes. In principle, this is doable via the optical spring effect, but would require local addressing with independent laser beams. This could prove challenging in a micron-scale photonic crystal architecture, severely hampering scalability.

Instead, we propose to employ frequency-selective operations, by modulating the laser intensity (and thus J) in a time-dependent fashion. Entanglement generation by parametric driving has been analyzed recently in various contexts, including entanglement using superconducting circuits [15], trapped ions [16], general studies of entanglement in sets of harmonic oscillators [17–19], optomechanical state transfer and entanglement between the motion of a trapped atom and a mechanical oscillator [20] and entanglement between mechanical and radiation modes [21]. Parametric driving can also lead to mechanical squeezing in optomechanical systems [22].

Let us consider two modes (1 and 2) for the moment, where the coupling is $2\hbar J(t)(\hat{X}_1 + \hat{X}_2)^2$. Assuming a 100% amplitude modulated laser drive beam with $|\alpha(t)|^2 = |\alpha_{\max}|^2 \cos^2(\omega t)$, we have $J(t) = J\cos^2(\omega t) = J[1 + \cos(2\omega t)]/2$. The resulting time-dependent light-induced mechanical coupling can be broken down into several contributions, whose relative importance will be determined by the drive frequency ω. The static terms, $\hbar J(\hat{X}_1 + \hat{X}_2)^2$, will shift the oscillator frequencies by $\delta\Omega_j = 2J$. In addition, they give rise to an off-resonant coupling (ineffective for $|\Omega_1 - \Omega_2| \gg J$, but with growing influence for $|\Omega_1 - \Omega_2| \lesssim J$). On the other hand, the oscillating terms contain

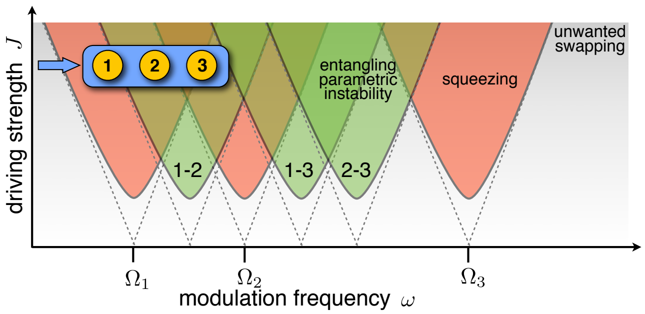

Figure 2: Squeezing and entanglement operations between three vibrational modes (Ω_1, Ω_2 and Ω_3) in an optomechanical setup, induced by harmonically modulating the laser intensity at a frequency ω. This schematic diagram shows the resonance regions for different processes starting to overlap when the effective light-induced coupling J is increased by changing the laser modulation amplitude ($J_{\mathrm{overlap}} = (\Omega_2 - \Omega_1)/2$ at first intersection of dashed lines). At large J the static part of the coupling also leads to unwanted swapping processes.

$$\hbar J(e^{2i\omega t} + e^{-2i\omega t})(\hat{b}_1 + \hat{b}_1^\dagger)(\hat{b}_2 + \hat{b}_2^\dagger). \tag{4}$$

There are three important cases. A mechanical beam-splitter (state-transfer) interaction is selected for a laser drive modulation frequency $\omega = (\Omega_1 - \Omega_2)/2$. After transforming the full Hamiltonian into the interaction picture with respect to Ω_1 and Ω_2, the resonant part then reads $\hat{H}_{\mathrm{b.s.}} = \hbar J(\hat{b}_2^\dagger \hat{b}_1 + \hat{b}_1^\dagger \hat{b}_2)$. In contrast, for $\omega = (\Omega_1 + \Omega_2)/2$, we obtain a two-mode squeezing (non-degenerate parametric amplifier) Hamiltonian, $\hat{H}_{\mathrm{ent}} = \hbar J(\hat{b}_1 \hat{b}_2 + \hat{b}_1^\dagger \hat{b}_2^\dagger)$, which can lead to efficient entanglement between the modes. Finally, $\omega = \Omega_j$ selects the squeezing interaction for a given mode, $\hat{H}_{sq} = \hbar(J/2)(\hat{b}_j^2 + \hat{b}_j^{\dagger 2})$. These laser-tunable, frequency-selective mechanical interactions are the basic ingredients for the architecture that we will develop and analyze here.

Limiting factors. – We now start to address the important constraining factors limiting the fidelity of these operations, both for the two-mode and ultimately the multi-mode case. Full simulations incorporating all these effects will be discussed further below. At higher drive powers (as needed for fast operations), the frequency-time uncertainty implies that the different processes discussed above need not be resonant exactly any more, with an allowable spread $|\delta\omega| \lesssim J$. For example, the parametric instabilities occur for $|\omega - (\Omega_i + \Omega_j)/2| < J$. At higher driving strengths, once these intervals start to overlap for different processes, selectivity is lost and the process fidelity suffers. On the other hand, at low operation speeds quantum dissipation and thermal fluctuations will limit the fidelity. This dilemma is the essential problem faced by a multi-mode setup, and we will discuss possible schemes to address it further below. The schematic situation for three modes is illustrated in Fig. 2.

In order to analyze quantitatively the full effects of decoherence and dissipation, we employ a Lindblad master equation to evolve the joint state of the mechanical modes under the influence of light-induced time-dependent driving. The evolution of any expectation value can be derived from the master equation and is governed by:

$$\begin{aligned}\frac{d}{dt}\left\langle \hat{A}\right\rangle &= \frac{1}{i\hbar}\left\langle [\hat{A},\hat{H}]\right\rangle + \sum_j (\bar{n}_j+1)\Gamma_j \left\langle \mathcal{R}[\hat{b}_j^\dagger]\hat{A}\right\rangle \\ &\quad + \sum_j \bar{n}_j\Gamma_j \left\langle \mathcal{R}[\hat{b}_j]\hat{A}\right\rangle .\end{aligned}$$

Here $\hat{H}$ already contains the effective interaction (3), with modulated time-dependent couplings, Γ_j are the mechanical damping rates of the vibrational modes, and $\bar{n}_j$ their equilibrium occupations at the bulk temperature. The dissipative term in the first line describes damping (spontaneous and induced emission), and the second line refers to absorption of thermal fluctuations. The relaxation superoperators are defined by $\mathcal{R}[\hat{b}^\dagger]\hat{A} = \hat{b}^\dagger\hat{A}\hat{b} - \hat{b}^\dagger\hat{b}\hat{A}/2 - \hat{A}\hat{b}^\dagger\hat{b}/2$ (in contrast to the equation for $\hat{\rho}$). For the quadratic Hamiltonian studied here, the equations for correlators, such as $\left\langle \hat{b}_i^\dagger \hat{b}_j\right\rangle$, remain closed, and these (together with averages $\left\langle \hat{b}_j\right\rangle$) are sufficient to describe the time-evolution of the Gaussian quantum states that will be produced in the course of the dynamics.

In order to analyze selective entanglement, we evaluate the logarithmic negativity

$$E_{\mathcal{N}}(\hat{\rho}) = \log_2 \left\| \hat{\rho}_{AB}^{T_A} \right\|_1 \tag{5}$$

as a measure of entanglement for any two given modes (A and B), where $\hat{\rho}_{AB}$ is the state of these two modes, and the partial transpose T_A acts on A only. For Gaussian states, $E_{\mathcal{N}}$ can be calculated by obtaining the symplectic eigenvalues of the covariance matrix of the two modes' positions and momenta [23].

In Fig. 3 we show the results of numerical simulations for a situation with three vibrational modes, two of which are to be entangled in the presence of the third one. The entanglement first grows and then saturates at later times, while the phonon number continues to grow exponentially. The plots show the entanglement evaluated at a fixed late time ($t = 5.6/J$), as a function of parameters. One clearly sees the features predicted above, i.e. the unwanted overlap between different entanglement processes at higher driving strengths (Fig. 3a,b). Increasing the vibrational frequency spacing suppresses these unwanted effects (Fig. 3b). The dependence on the driving strength itself is displayed in more detail in Fig. 3c. There, the threshold $J = \Gamma\bar{n}$ for entanglement generation at finite temperature is evident, as is the loss of entanglement at large J. Finally, Fig. 3d,e shows the dependence on temperature and mechanical quality factor. It indicates that this scheme should be feasible for realistic experimental parameters (see below). Note that the light-induced dissipation [24] effectively adds to the intrinsic decoherence rate $\Gamma\bar{n}$ the rate $\Gamma_{\rm opt}^{\varphi} \approx g_0^2\alpha^2\kappa/\Delta^2 = 2J(\kappa/\Delta)$. This is suppressed by a factor κ/Δ which can in principle be made arbitrarily small for larger detuning (at the expense

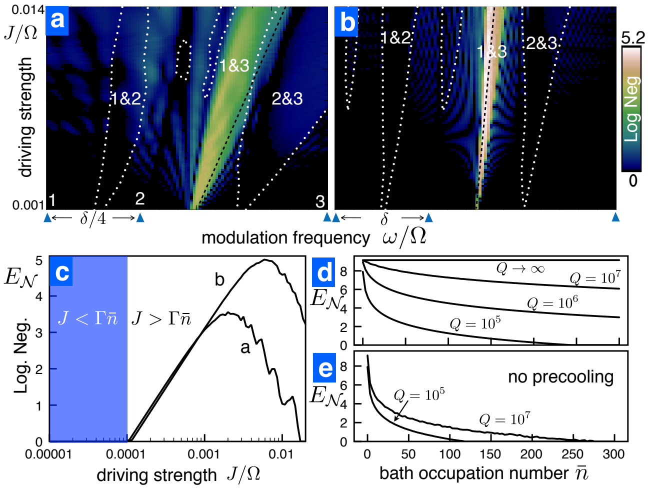

Figure 3: Selective entanglement between two vibrational modes, in an array of three, produced by an amplitude-modulated laser beam driving a common optical mode. All modes are coupled to a thermal bath and assumed to be cooled to their ground state via side-band cooling prior to the entanglement operation. (a,b) Color plots showing an entanglement measure (the logarithmic negativity) between modes 1 and 3, as a function of the driving strength J and the modulation frequency ω, at a fixed time. In (a) the vibrational modes are quite close [$\Omega_i = (1, 1.025, 1.075)\Omega$], which leads to overlapping resonance regions for different processes (as in Fig. 2). In (b), the frequency spacing is increased by a factor of four, significantly increasing the selectivity. (c) Dependence on driving strength, i.e. cut along lines indicated in (a,b), see main text. (d) Dependence on temperature and mechanical quality factor. (e) Same as (d) but without precooling, i.e. starting from thermal equilibrium. [Contour lines in (a,b): entanglement between 1&2 or 2&3 larger than 1.0, blue arrows at Ω_j; Parameters for (a,b,c): $\bar{n} = 100$, $Q = 10^6$; (d,e): $J/\Omega = 0.003$; (b,d,e): $\Omega_i = (1, 1.1, 1.3)\Omega$]

of higher circulating photon number α^2 to keep the same J). For the realistic experimental parameters quoted below, we have $\kappa/\Delta = 1/80$, such that we have been able to neglect the effects of $\Gamma^{\varphi}_{\rm opt}$.

Larger arrays. – We now turn to the situation with an array of many modes. It is clear that having evenly spaced mechanical frequencies is impossible without taking any further precautions. This is because then the state transfers between adjacent modes would all be addressed at the same modulation frequency. In fact, there seems to be no layout that allows for selection of arbitrary pairs, avoids resonance overlap, and does not require a frequency interval that grows exponentially with the number N of modes. While one may still realize small arrays in this way, in the limit of large N another approach is needed.

The scheme (Fig. 4) that solves this challenge involves an auxiliary mode at $\Omega_{\rm aux}$, removed in frequency from the array of "memory" modes which now may have evenly spaced frequencies in an interval $[\Omega_{\rm min}, \Omega_{\rm max}]$. All the pairwise operations will take place between any selected memory mode and the auxiliary mode. Then, the state transfer resonances are in the band $[(\Omega_{\rm aux} - \Omega_{\rm max})/2, (\Omega_{\rm aux} - \Omega_{\rm min})/2]$, and entanglement is addressed within $[(\Omega_{\rm min} + \Omega_{\rm aux})/2, (\Omega_{\rm max} + \Omega_{\rm aux})/2]$. To make this work, one needs to fulfill the mild constraint $2\Omega_{\rm max} - \Omega_{\rm min} < \Omega_{\rm aux} < 3\Omega_{\rm min}$. State transfer between two memory modes now is performed in three steps (swapping 1–aux, aux–2 and aux – 1), as is entanglement (swap 1–aux, entangle aux–2 and swap aux–1). Note that this overhead does not grow with the number of memory modes. Fig. 5 shows the state transfer between an auxiliary mode (originally prepared in a squeezed state) and one of the memory modes. This scheme can potentially be expanded, with the auxiliary modes grouped into arrays (Fig. 4c), and several of such 2D blocks could again be connected via further "higher-order" auxiliary modes, in a hierarchical fasion.

Implementation. – Regarding the experimental implementation, in principle any optomechanical system with several long-lived mechanical modes can be used as a starting point. One promising platform is based on photonic crystals ("optomechanical crystals"), as introduced by Painter et al. [2]. These would be very well suited for the scheme presented here, due to their design flexibility, particularly of two-dimensional structures, and the all-integrated approach, as well as the very large optomechanical coupling strength. Given the current coupling strength achieved there [8], $g_0/2\pi \sim$ 1MHz, as well as a detuning of $\Delta/\Omega = 10$ and around 2000 photons circulating inside the cavity (a number reached in recent experiments), we can estimate the induced coupling to approach the damping rate, $J \sim \Gamma$. This corresponds to the threshold for coherent operations, provided one were to cool down the bath to $k_B T_{\rm bath} < \hbar\Omega$. This is in principle doable (at 20mK), but will likely run into practical difficulties due to the re-heating of the structure via spurious photon absorption or other effects. Otherwise, at finite bath temperatures corresponding to a thermal occupation $\bar{n} \sim k_B T_{\rm bath}/\hbar\Omega$, the light intensity must be increased by a factor $\bar{n}$, towards $J \gg \Gamma\bar{n}$, to speed up operations and thereby fight thermal decoherence. In that case, the vibrational ground state would be prepared at the start of the pulse sequence via laser-cooling, as demonstrated in [8].

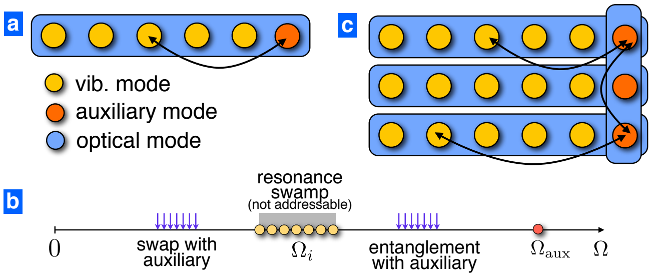

Figure 4: (a) Layout for an optomechanical array with an auxiliary vibrational mode, circumventing the problem of frequency crowding (see main text). (b) Corresponding mechanical frequency spectrum. The laser modulation frequency has to lie within certain intervals to select entanglement or state-transfer operations between the "memory modes" and the auxiliary mode. (c) Extension to the second dimension with operations "around the corner".

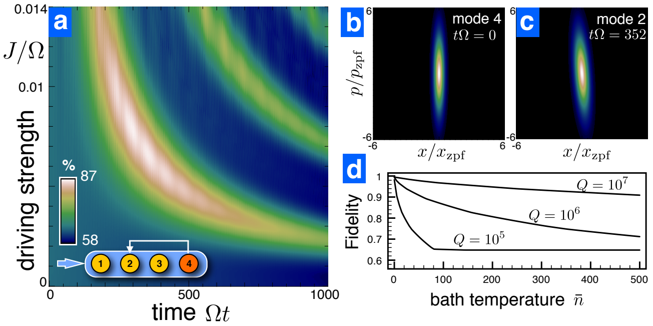

Figure 5: State transfer of a squeezed state ($\Delta x^2 = e^{-2} x^2_{\rm ZPF}$) from the auxiliary to the second memory mode (all in the ground state due to prior side-band cooling) (a) Dependence of the transfer fidelity on driving strength and pulse time, with a swap pulse ideally occuring at $Jt = \pi/2$. For long pulse times dissipation hampers the transfer, for large driving strengths resonances overlap, medium times are optimal. (b) Wigner density of the initial squeezed state in the auxiliary mode, and (c) after the transfer. (d) Maximization of transfer fidelity over parameter ranges used in (a). Parameters: $\Omega_j = (1.0, 1.1, 1.2, 2.0)\Omega$, $\bar{n} = 100$, $Q = 10^6$,$J/\Omega = 0.007$ (b,c).

In these devices, several localized vibrational and optical modes can be produced at engineered defects in an otherwise periodic array of holes cut into a free-standing substrate (e.g., made of silicon). Evanescent optical and vibrational waves connect adjacent modes (via photon and phonon tunneling, respectively). The typical photon tunnel coupling for modes spaced apart by several lattice constants is [4] in the range of several THz. Thus, hybridized optical modes will form, one of which can be selected via the laser driving frequency as the active common optical mode (the others remaining idle). At the same time, the vibrational modes' frequencies can either be designed to be different or to be equal, in which case delocalized hybridized mechanical modes are produced. Recently it was shown that a 'snowflake' crystal made of connected triangles (honeycomb lattice) possesses a simultaneous photonic and phononic (pseudo-)bandgap and thus supports wave guides (line defects) and localized defect modes with optomechanical interaction [3]. Placing point defects (heavier triangles/thicker bridges) in the middle of such a crystal structure, a tight binding analysis indicates that the desired mechanical frequency spectrum (Fig. 4) can be generated in principle.

In any given system there will be limits to the design of the mechanical spectrum. We briefly mention another option for improving the operational fidelity: pulse shaping and optimal control. Essentially, one wants to make sure that the Fourier transform of the coupling $J(t)$ (or, equivalently, of the time-dependent laser intensity), does not contain spectral weight at any of the resonances $\omega_{ij}^{\pm} = (\Omega_i \pm \Omega_j)/2$, except for the selected one. This implies that the pulse duration is larger than the inverse of the smallest spacing of such resonances. Optimal control techniques (as in [17]) could be employed to numerically search for the optimal pulse shape.

Finally, one essential ingredient of any such architecture will be read-out. Some time ago, we have pointed out [25] how to produce a quantum-non-demolition readout of the quadratures of mechanical motion in an optomechanical setup. A laser beam impinging onto the optical resonance (detuning $\Delta = 0$) is amplitude-modulated at the mechanical frequency Ω_j of one of the modes. The reflected light carries information only about one quadrature $e^{i\varphi}\hat{b}_j + e^{-i\varphi}\hat{b}_j^{\dagger}$. Its phase φ is selected by the phase of the amplitude-modulation, while the measurement backaction perturbs solely the other quadrature. In that way, by repeated measurements all the joint correlators of positions and momenta of the mechanical modes may be read out, e.g. in order to verify the fidelity of the operations discussed above. If desired, taking measurement statistics for continuously varied quadrature phases would also allow to do full quantum-state tomography of the set of vibrational modes, and thereby ultimately process tomography.

Conclusions. – The scheme described here would enable coherent scalable nanomechanical state processing in optomechanical arrays. It can form the basis for generating arbitrary entangled mechanical Gaussian multi-mode states. An interesting application would be to investigate the decoherence of such states due to the correlated quantum noise acting on the nanomechanical modes. Moreover, recent experiments have shown in principle how arbitrary states can be written from the light field into the mechanics [5–7]. These could then be manipulated by the interactions described here. Alternatively, for very strong coupling $g_0 > \kappa$, non-Gaussian mechanical states [26] could be produced, and the induced nonlinear interactions (see e.g. [27, 28]) could potentially open the door to universal quantum computation with continuous variables [9] in these systems.

We acknowledge an ERC Starting Grant, the DFG Emmy-Noether program and DARPA ORCHID for funding.

---

[1] F. Marquardt and S. Girvin, Physics **2**, 40 (2009).

[2] M. Eichenfield, J. Chan, R. M. Camacho, K. J. Vahala, and O. Painter, Nature **462**, 78 (2009).

[3] A. H. Safavi-Naeini and O. Painter, New J. Phys. **13**, 013017 (2011).

[4] G. Heinrich, M. Ludwig, J. Qian, B. Kubala, and F. Marquardt, Phys. Rev. Lett. **107**, 043603 (2011).

[5] A. H. Safavi-Naeini, T. P. Mayer Alegre, J. Chan, M. Eichenfield, M. Winger, Q. Lin, J. T. Hill, D. Chang, and O. Painter, Nature **472**, 69 (2011).

[6] V. Fiore, Y. Yang, M. C. Kuzyk, R. Barbour, L. Tian, and H. Wang, Phys. Rev. Lett. **107**, 133601 (2011).

[7] E. Verhagen, S. Deléglise, S. Weis, A. Schliesser, and T. J. Kippenberg, Nature **482**, 63 (2012).

[8] J. Chan, T. P. M. Alegre, A. H. Safavi-Naeini, J. T. Hill, A. Krause, S. Groeblacher, M. Aspelmeyer, and O. Painter, Nature **478**, 89 (2011).

[9] S. L. Braunstein and P. van Loock, Rev. Mod. Phys. **77**, 513 (2005).

[10] M. Pinard, A. Dantan, D. Vitali, O. Arcizet, T. Briant, and A. Heidmann, EPL **72**, 747 (2005).

[11] D. Vitali, S. Gigan, A. Ferreira, H. R. Böhm, P. Tombesi, A. Guerreiro, V. Vedral, A. Zeilinger, and M. Aspelmeyer, Phys. Rev. Lett. **98**, 030405 (2007).

[12] M. J. Hartmann and M. B. Plenio, Phys. Rev. Lett. **101**, 200503 (2008).

[13] K. Hammerer, M. Wallquist, C. Genes, M. Ludwig, F. Marquardt, P. Treutlein, P. Zoller, J. Ye, and H. J. Kimble, Phys. Rev. Lett. **103**, 063005 (2009).

[14] M. Ludwig, K. Hammerer, and F. Marquardt, Phys. Rev. A **82**, 012333 (2010).

[15] L. Tian, M. S. Allman, and R. W. Simmonds, New J. Phys. **10**, 115001 (2008).

[16] A. Serafini, A. Retzker, and M. B. Plenio, New J. Phys. **11**, 023007 (2009).

[17] F. Galve and E. Lutz, Phys. Rev. A **79**, 032327 (2009).

[18] V. M. Bastidas, J. H. Reina, C. Emary, and T. Brandes, Phys. Rev. A **81**, 012316 (2010).

[19] F. Galve, L. A. Pachón, and D. Zueco, Phys. Rev. Lett. **105**, 180501 (2010).

[20] M. Wallquist, K. Hammerer, P. Zoller, C. Genes, M. Ludwig, F. Marquardt, P. Treutlein, J. Ye, and H. J. Kimble, Phys. Rev. A **81**, 023816 (2010).

[21] A. Mari and J. Eisert, arXiv:1111.2415 (2011).

[22] A. Mari and J. Eisert, Phys. Rev. Lett. **103**, 213603 (2009).

[23] G. Vidal and R. F. Werner, Phys. Rev. A **65**, 032314 (2002).

[24] F. Marquardt, J. P. Chen, A. A. Clerk, and S. M. Girvin, Phys. Rev. Lett. **99**, 093902 (2007).

[25] A. A. Clerk, F. Marquardt, and K. Jacobs, New J. Phys. **10**, 095010 (2008).

[26] J. Qian, A. A. Clerk, K. Hammerer, and F. Marquardt, arXiv:1112.6200 (2011).

[27] M. Ludwig, A. H. Safavi-Naeini, O. Painter, and F. Marquardt, arXiv:1202.0532 (2012).

[28] K. Stannigel, P. Komar, S. J. M. Habraken, S. D. Bennett, M. D. Lukin, P. Zoller, and P. Rabl, arXiv:1202.3273 (2012).